A. S. Argon, J. G. Hannoosh and M. M. Salama

Fracture 1977, Volume 1, ICF4, Waterloo, Canada, June 19 - 24, 1977

INITIATION AND GROWTH OF CRAZES IN GLASSY POLYMERS

A. S. Argon*, J. G. Hannoosh**, and M. M. Salama***

ABSTRACT

In glassy polymers crazes initiate at surface or interface stress concentrations where localized plastic flow produces microcavities by intense inhomogeneous plastic shear at a molecular scale. The rate of such cavity formation depends primarily on the local concentrated deviatoric stress while their subsequent plastic expansion into craze nuclei by their mutual interaction is in response to the global negative pressure. Once a craze nucleus forms into a spongy heterogeneity of significant aspect ratio it grows by the meniscus instability in which new craze matter, having continuously interconnected air passages, forms by the repeated convolutions of the concave interface of air and yielded polymer at the craze tip. The proposed theory not only gives quantitative agreement with the experimental measurements on the rates of initiation and growth of crazes at room temperature and below, but also predicts the scale factor of the structure of craze matter.

INTRODUCTION

Crazing in glassy polymers has long been known to play a dual role. When their initiation and growth is carefully controlled, as in the case of multi-phase high impact polystyrene (HIPS) and acrylonitrile-butadiene-styrene (ABS) polymers, crazes can be a source of toughness. On the other hand, in most single-phase glassy polymers crazes are precursors to fracture. The phenomenology of crazing is rich in detail for which the reader is referred to recent comprehensive reviews [1,2]. Here we will concentrate only on the mechanisms and kinetics of the nucleation and growth of crazes in single phase, unoriented glassy polymers under normal dry conditions.

Maxwell and Rahm [3] were the first to study the kinetics of nucleation of crazes from surfaces of stressed polystyrene (PS) and polymethyl methacrylate (PMMA). They were also the first to emphasize the key role of surface stress concentrations and effect of solvents in accentuating crazing. Following the clarification of the important role of crazing in the toughness of rubber modified polymers by Bucknall and Smith [4] interest in crazing was concentrated on: the development of phenomenological stress or strain criteria for so-called craze-yielding [5-10]; and on consideration of crazes as the source of plastic dissipation in the crack propagation process in dry polymers [11,12], and in solvent crazing both in the presence of fluids [13-17], and in the presence of gases [18,19]. In addition, however, the structure [20,21] and mechanical behavior of craze matter [22,23] received attention, the effect of molecular weight on the structure of craze

*Department of Mechanical Engineering, M.I.T. Cambridge, Mass. U.S.A.
**Foster, Miller Associates, Waltham, Mass. U.S.A.
***Stone and Webster Engineering Corp., Boston, Mass.

matter was studied [24-26], and some recognition was given to the source of scatter [17,27] in the crazing phenomenon. Although much useful quantitative detail became known as a result of these studies, the mechanisms of initiation of craze nuclei and craze matter production remained speculative. Gent [28], for example, theorized that crazing requires a devitrification of the glassy polymer into a rubbery state by the enhanced negative pressure at stress concentrations, which was then to produce cavitation in the rubber by an unspecified mechanism. It is generally [29,30] appreciated that since crazing stresses are about within a factor of three of the yield stress, the very large stress concentrations which this mechanism requires can never be present in a polymer and therefore this process cannot occur. Another, and more specific mechanism for crazing was proposed by Argon [29, 33] in which precursor micropores are nucleated by the stress concentrations of inhomogeneous plastic deformation on a scale of the order of 50-100. A, this is followed by their plastic expansion in the already yielded material under the action of the negative pressure existing in the stress field. This occurs when the porosity reaches a critical value that depends on the negative pressure by well-known continuum plasticity solutions of cavity expansion. This model is consistent with the extensive experiments of Zhurkov and co-workers [31,32] on micropore formation in stressed polymers by a thermally activated process and some of its details have been verified by direct observation in thin films in the electron microscope [25,26]. In addition, preliminary experiments that have been reported earlier [33] have furnished confirmation for the theory. Here we will give a summary of more extensive recent experiments [34] on the kinetics of the nucleation of crazes that demonstrate the correctness of the proposed mechanism.

The kinetics of growth of crazes has also received attention. Apart from the pioneering experiments of Bessonov and Kuvshinskii [35] and some isolated modern studies [36-37], on the growth of dry crazes, however, most current studies have concentrated on the growth of crazes in the presence of solvents [15-17,38]. A Fourier transform solution for stress distribution along a craze in an elastic surrounding was obtained by Knight [39] in which the extension criterion for the craze is a critical "craze initiation stress" at the tip. This solution, however, has many characteristics that are hard to justify [30]. On the other hand, planar yield zone solutions have been more successful in accounting for craze growth velocities. Such solutions usually assume: either a critical craze tip opening displacement [16]; a critical energy release rate (or cavitation work) [15]; or a critical craze tip wedge angle, and obtain craze growth by time dependent stress relaxation of the craze matter. Only Andrews and Bevan [15] have suggested a specific mechanism, which in their case involves elastic-plastic expansion of cavities whose mode of formation was left unspecified. On the other hand, Argon [29] has initially suggested that crazes grow by repeated nucleation of pores ahead of the main craze due to the same inhomogeneous plastic flow processes that are responsible for the formation of the main craze nucleus, when the local conditions at the tip of the craze reach the nucleation condition. Further examination of this proposal, however, showed shortcomings: first the stress intensification at the craze tip is not very suitable for pore formation [40], and second, the nucleation of isolated pores leads to a topologically different craze structure from that of craze matter in which the "vacant phase" is continuously interconnected. For this reason it was proposed [33] that craze matter forms by the mechanism of the "meniscus instability", in which the yielded polymer at the air-polymer interface at the craze tip, that is basically unstable to perturbations of a well-defined wavelength, breaks up, and by repeated convolutions produces the topologically correct form

of craze matter in a continuous manner. Here we will give a summary of the theoretical modelling of this mechanism of craze growth and present experimental results that are in agreement with it.

THEORY

Formation of craze nuclei

In their pioneering studies Zhurkov and co-workers have observed thermally activated pore formation in many stressed crystalline and glassy polymers [31]. It is well known that nucleation of pores in a continuous homogeneous material is exceedingly difficult, and requires reaching negative pressures that are very nearly equal to the cohesive strength of the material whereupon the material becomes unstable and expands uncontrollably. Since this is not what occurs in polymers, it is clear that neither the state of stress nor the inelastic strains are homogeneous in even the most homogeneous appearing glassy polymers. Formation of pores requires inhomogeneous plastic flow, albeit at a molecular level; and relatively stable retention of porosity requires inhomogeneous distribution of stress, i.e. stress concentrations. It was for these reasons that the localized microshear process in Figure 1 (well known in crystal plasticity as the Stroh [41] mechanism) was proposed for pore formation [33]. The activation free energy ΔG^* for the formation of such a slip nucleus under a shear stress τ was obtained to be

$$\Delta G^* = (0.15)^2 \pi(\mu/\tau)(\mu\phi^3) \tag{1}$$

where μ is the athermal shear modulus of the polymer at the given temperature and ϕ is the relative displacement across the sheared region (usually a molecular dimension characteristic of the polymer, such as the molecular diameter). It was shown further that although the critical radius of the slip patch is only of the order of 4ϕ, once formed, the patch may expand under falling local stress to a size L governed by the distance of molecular heterogeneities. When arrested it has then enough concentration of local normal stress and enough local strain energy to provide for the surface free energy of at least one micro-crack. Forming a stable, round cavity, however, requires some additional plastic deformation with expenditure of work of the order of $\alpha L^3 Y$, where Y is the yield strength of the polymer and α a factor or order 0.1. Thus, the formation of a round pore will require a total free energy of

$$\Delta G^*_{pore} = (0.15)^2 \pi(\mu/\tau)(\mu\phi^3) + \alpha L^3 Y \tag{2}$$

It must be emphasized that this relatively coarse mode of plastic flow described above, as well as its free energy for formation (1), are fundamentally different from the more local mechanism of plastic flow in glassy polymers by the thermally activated rotation of segments of molecules described in detail by Argon [42].

Under a multi-axial state of stress, and in consideration of the molecular heterogeneities, the shear stress τ is interpreted as the *local* deviatoric stress s (for a definition of s, see [42]) existing at a stress concentration, that is nearly always a surface groove, but can also be a protuberance on a dust particle or a latex occlusion in a rubber modified polymer. Neuber [43] has considered in detail the stress concentrating effect of surface grooves under any general state of stress shown in Figure 2. The concentrated local stress σ_{11}, σ_{22}, and σ_{12} are according to Neuber (for a Poisson's ratio of 0.5 where yielding begins)

$$\hat{\sigma}_{22} = \sigma_{22}\ (1 + 1.296k) \tag{3a}$$

$$\hat{\sigma}_{11} = \sigma_{11} + 0.600\ \sigma_{22}k \tag{3b}$$

$$\hat{\sigma}_{12} = \sigma_{12}\ (1 + 0.365k) \tag{3c}$$

where σ_{11}, σ_{22}, and σ_{12} are the applied stresses and $k = (a/b)$ is the aspect ratio of the groove considered to be a half ellipse. It can be shown [34,44] that for a randomly oriented set of grooves of constant aspect ratio (in the range $K \lesssim 5$), the groove for which the deviatoric stress is largest is that which is normal to the maximum principal tensile stress σ_2. Hence, in any real situation where grooves of random orientation exist on the surface it is only this deviatoric stress that is of interest which can be computed readily to be

$$s = Y\left[0.333(\eta - \xi)^2 + (0.032k + 0.333)(\eta^2 - \xi^3) + (0.421k^2 + 0.664k + 0.333)(\eta + \xi)^2\right]^{1/2} \tag{4}$$

where

$$\eta = (\sigma_2 - \sigma_1)/2Y \tag{5a}$$

$$\xi = (\sigma_2 + \sigma_2)/2Y \tag{5b}$$

and where Y the yield stress of the polymer (at a conventional strain rate such as 10^{-4}sec^{-1}) at the required temperature is used as a convenient normalization parameter.

It can then be assumed that the local porosity β, at the roots of surface grooves increases with time according to the expression

$$\beta = \dot{\beta}_o t\ \exp(-\Delta G^*_{\text{pore}}(s)/kT) \tag{6}$$

where $\dot{\beta}_o$ is a frequency factor characteristic of the vibration of a region of the order of the critical radius of the activated configuration ($\sim 4\phi$).

Figure 3 shows such a porous region of radius r_o at the root of a surface groove having roughly the same radius of curvature. To make the problem no more complicated than necessary it can be assumed that the material in this region is rigid plastic and it is at a state of plastic flow while the material outside is elastic. It can be expected further that the thermally activated production of this porosity has relieved the local concentration of negative pressure so that any plastic expansion resulting from the interaction of such pores can be accomplished only under the action of the background (global) negative pressure. It is readily shown [29] that if the material had not already been brought to a state of flow by the local deviatoric stress s, the negative pressure σ that is required to plastically expand the process region is $(2Y/3)(\ell n(1/\beta))$. When the material is already at a state of flow, however, the required negative pressure is very much reduced. McClintock and Stowers [45] have recently given loci of σ and s for the plastic expansion of such porous regions, for different levels of porosity β. Based on this work the negative pressure σ for expansion of porous regions can be written as

$$\sigma = \frac{2Y}{3}\ [\ell n(1/\beta)]\,[Q(s/Y,\beta)] \tag{7}$$

where $Q(s/Y,\beta)$ is a normalized locus for pore expansion which is shown in Figure 4 for a porosity of $\beta = 0.01$. Clearly, when the material is nearly at a state of yield, Q, and therefore, the required σ are very small, but so is the rate of expansion of the pores. In practice, the actual level of Q will be governed by the rate sensitivity of the material.

In previous descriptions of the theory of craze nucleation [29, 33] it was stated that the plastic expansion of pores by elastic unloading of the surroundings requires a negative pressure exceeding a critical amount. This condition that was derived for a porous material that has not been previously brought to a state of flow by the presence of a large deviatoric stress is completely relaxed when the material is already at a state of flow.

Equations (6) and (7) together give the time t_{in} after which the craze nucleus formation by plastic interaction of the already formed pores begins under a local deviatoric stress s and a background negative pressure σ:

$$t_{in} = (1/\dot{\beta}_o)\ \exp\left[(\Delta G^*_{\text{pore}}/kT) - (\xi/Q)\right] \tag{8}$$

where ξ was defined by equation (5b).

Additional time will, however, be required to expand pores by elastically unloading the surroundings before a craze nucleus becomes of visible size. An estimate of this growth time can be obtained by considering a phenomenological, power-law form for the relationship between effective strain rate $\dot{\varepsilon}_e$ and effective stress σ_e ($\sigma_e = \sqrt{3}\,s$) i.e. $(\dot{\varepsilon}_e/\dot{\varepsilon}_o) = (\sigma_e/\sigma_o)^m$ where $\dot{\varepsilon}_o$, σ_o, and m are phenomenological, temperature dependent constants of the material. It can then be shown [44] that the additional time for growth of pores under the background negative pressure σ is

$$\Delta t_{\text{growth}} = (2/3\dot{\varepsilon})\,(mQ/\xi)^m \int_{\beta_i}^{\beta_f} \left[(1-\beta^{1/m})^m/\beta(1-\beta)\right]\ d\beta \tag{9}$$

where β_i (~ 0.005) the initial porosity given by equation (6) where growth commences and β_f (~ 0.1) is the final porosity where the nucleus is large enough to scatter light. Thus, the total time for formation of a visible craze nucleus will be the sum of the times given by equations (8) and (9), as

$$t(\text{craze nucleation}) = t(\text{initiation}) + \Delta t(\text{growth}) \tag{10}$$

As is apparent from equation (9) the growth time makes up a significant fraction of the total only when the background negative pressure is very small. In pure shear where $\sigma = 0$ craze nuclei cannot form even though much micropore formation will take place.

It can be assumed that surfaces of commercial polymers have a family of randomly positioned microgrooves (scratches). Experience (and experiments to be discussed below) suggest that the surface density N and severity k of such grooves are distributed approximately according to a normal distribution function as

$$N = N_o\left[1 - (1/\sqrt{2\pi}) \int_{-\infty}^{(k-\bar{k})/\sigma_k} \exp\left(-\frac{\zeta^2}{2}\right) d\zeta\right] \tag{11}$$

where N_o is the total number of grooves (normal to the maximum principal tensile stress) per unit area on the surface, $\bar{k}$ the mean aspect ratio of the distribution of grooves, and σ_k the standard deviation of this aspect ratio. The local deviatoric stress s depends on k: hence, the initiation times t_{in} of grooves become progressively longer as k decreases, and the observed increase in the surface density of craze sites with time under constant stress reflects directly the operation of this stress on the spectrum of surface grooves [33,17].

Under a constant state of stress crazing eventually ceases at an apparent saturation density of crazes that increases with increasing levels of applied stress [6,33]. This occurs when the previously nucleated crazes have grown enough to interfer with each other and also unload other potential crazable sites at which the craze nucleation condition has not yet been met. This condition of craze saturation can be expected to be satisfied when a certain fraction f of the entire surface is covered by crazes. This fraction f is given by

$$f = 2\pi \left(\frac{da}{dt}\right)^2 \int_{N(k)}^{N(k_{sat})} \left(t(k_{sat}) - t(k)\right)^2 dN \tag{12a}$$

$$f = \frac{\sqrt{2\pi}\, N_o}{\beta_o^2} \left(\frac{da}{dt}\right)^2 \exp(-2\xi/Q) \int_{k_{sat}}^{\infty} \left(\exp \frac{\Delta G^*_{pore}(s(k_{sat}))}{kT} - \exp \frac{\Delta G^*_{pore}(s(k))}{kT}\right)^2 \times \exp\left[-\left(\frac{k - \bar{k}}{\sqrt{2}\,\sigma_k}\right)^2\right] dk \tag{12b}$$

where a is the half-craze growth rate which, as will be discussed below, depends only on the maximum principal tensile stress. In equations (12a,12b) the growth time for pores, given in equation (9) was neglected.

Growth of Crazes

After a craze nucleus has formed at a surface groove, the stress at the site of the nucleus is reduced while it is increased around the periphery of the nucleus. In an isotropic polymer this will make the craze grow across the stress that can produce the largest opening displacement, i.e. across the maximum principal tensile stress. It is natural to expect that the mechanism of hole nucleation that gave rise to the craze nucleus will continue to add new craze matter to the already established nucleus at its most highly stressed periphery. As has been mentioned in the introduction, however, when quantitatively evaluated [40], such a mode of craze growth does not only fall short by orders of magnitude from accounting for the observed rate of growth of crazes and its stress dependence, but also gives a closed-cellular craze structure that is topologically different from the known craze structure in which the vacant phase (air gaps) is continuously connected. The mechanism that fits all requirements is one in which craze tufts are produced by the repeated break-up of the concave air-polymer interface at the craze tip as shown schematically in Figure 5. Such

convolution of the yielded polymer at the craze tip results from a basic instability of all fluid (whether linear or non-linear) menisci advancing under the action of a suction gradient created in the fluid [46]. This is because such interfaces are unstable to perturbations above a certain wavelength that decreases with an increasing suction gradient (negative pressure gradient).

To determine the rate of growth of an already established craze we consider it as a narrow discontinuity transmitting a normal traction σ_o that can as a first approximation be taken as Y/λ_n where λ_n is the natural draw ratio of the polymer in the craze matter and Y the tensile yield stress of the polymer. Under an applied tensile stress σ_∞ there will be a plastic zone of extent R (see Figure 6) at the tip of a craze of length 2a that is by elementary small scale yielding theory.

$$R = a\left(\frac{\sigma_\infty - \sigma_o}{Y - \sigma_o}\right)^2 \tag{13}$$

Upon such local yielding, the craze tip, which is considered to be free of surface traction, will blunt to a radius of curvature of R_c and then establish a steady state transverse corrugation with a wavelength λ, by the meniscus instability mechanism that will, by repeated convolutions, produce new craze tufts and advance the craze tip steadily forward as shown in the sketch of Figure 5. When the craze grows, a material point enters the plastic zone at the far end, advances in a field of intensifying plastic strain, and finally appears at the polymer-air interface ready for the interface convolution process that forms craze matter. Argon and Salama [46] have shown that the condition corresponds to a craze tip velocity of

$$\frac{da}{dt} = \frac{\delta \dot{\varepsilon}}{6} \tag{14}$$

where δ is the critical craze tip opening displacement at which a new increment of craze matter is added to the craze and $\dot{\varepsilon}$ is the plastic strain rate of a solid polymer corresponding to an applied stress Y and temperature T according to an expression given by the theory for the yield stress developed by Argon [42]. This gives for the craze growth rate upon substitution

$$\frac{da}{dt} = \frac{\delta}{6}\dot{\varepsilon}_o \exp\left\{-\frac{A}{T}\left[1 - \left(\frac{Y}{\hat{Y}}\right)^{5/6}\right]\right\} \tag{15a}$$

where

$$A = \frac{3\pi\mu\omega^2 b^3}{16(1-\nu)k} \tag{15b}$$

$$\hat{Y} = \frac{0.133}{(1-\nu)}\mu \tag{15c}$$

In equations (15a), (15b) and (15c) ω, and b are the angle or rotation of a segment of a molecule, or cluster of molecules, having a radius b, $\dot{\varepsilon}_o$ is a frequency factor ($0(10^{13})$) and k is Boltzmann's constant. Experimentally determined values for $\omega^2 b^3$ have been given by Argon and Bessonov [47] for a large group of glassy polymers. Argon and Salama [46] who have examined the described mode of craze growth by the meniscus instability find that the steady state craze opening displacement δ is given by

$$\delta = 24\pi^2\sqrt{3}\, B\,(1/m)\,\frac{X}{Y} \tag{16}$$

where χ is the surface tension of the polymer and B(1/m) is a function of the reciprocal of the phenomenological strain rate sensitivity exponent introduced above in connection with equation (9). For most polymers in which m ranges between 5-25 B(1/m) ranges from 10 down to 3 [46].

If a steady state growth exists for crazes in polymers with a relatively sharp elastic to plastic transition, it can be assumed that both the craze matter traction $\sigma_o = Y/\lambda_n$ as well as Y have the same strain rate and temperature sensitivity entering equation (15a), and that after a short transitional growth period, the extent of the plastic zone at the craze tip makes up an ever decreasing fraction of the craze length. As equation (13) then shows, this enables the craze to speed up to a final steady state velocity until σ_o rises to almost the level of σ_∞, and Y to $\lambda_n\sigma_\infty$. Equations (15a) and (16) then give the asymptotic (steady) velocity of mature crazes as

$$\frac{da}{dt} = \frac{D}{(\lambda_n\sigma_\infty/\hat{Y})} \exp\left\{-\frac{A}{T}\left[1 - \left(\frac{\lambda_n\sigma_\infty}{\hat{Y}}\right)^{5/6}\right]\right\} \qquad (17)$$

where $$D = \frac{24\pi^2\sqrt{3}\ B(1/m)\ \chi\dot{\varepsilon}_o}{\hat{Y}} \qquad (18)$$

Our development assumes that the traction across the faces of the established craze remains constant at σ_o. Since the relative displacement between faces must increase with increasing craze length and since the craze matter is known to undergo orientation hardening, it is necessary that some new polymer be drawn out from the faces at this constant level of traction. Most observations are in support of such craze broadening [2]. We note here in passing that the proposed mechanism for growth of dry crazes has several important features to explain accelerated growth of crazes in solvents. First the topology of the craze matter produced by the meniscus instability permits solvents to flow readily to the craze tip. Second, the presence of the solvent at the craze tip will accelerate growth by: a) reducing the surface energy [15], and b) dissolving into the polymer locally to reduce its modulus and thereby reducing both A and Y in equations (17) and (18) [15].

It is also worth noting that the presence of a second principal stress, algebraically smaller than the first, will produce only minimal changes on the growth rate given by equations (17) and (18). This is because the meniscus instability process that governs the rate of addition of craze matter is influenced primarily by the positive gradient of negative pressure at the tip of the craze which results from the craze tip blunting by plastic flow. This blunting, however, is a result of the maximum principal tensile stress alone, and is largely uninfluenced by the specific shape of the plastic zone that is known to depend on both principal stresses. Experiments discussed below confirm that under multi-axial stresses the craze growth rate depends only on the level of the maximum principal tensile stress.

EXPERIMENTS

Material and Experimental Procedure

Since the rate of craze initiation depends on the level of local deviatoric stress and the global negative pressure on the surface, it is essential not only to control these components of the stress tensor independently over a significant range but also control the degree of surface roughness. For these reasons the crazing experiments were conducted on specially

manufactured tubular specimens having a central, thin walled hour-glass section that could be subjected to combined tension and torsion, making possible a controlled variation of the global stress from pure deviatoric (i.e., $\sigma/s = 0$) to pure tension (i.e., $\sigma/s = 1\sqrt{3}$). As discussed in more detail elsewhere [34,44], the specimens were precision machined from annealed blocks made by pressure molding of Dow 686 grade atactic polystyrene pellets [*] at 165°C and 7.58 MPa. Gel permeation chromatography gave a number average molecular weight of $M_n = 8.95 \times 10^4$ and a weight average molecular weight of $M_w = 3.36 \times 10^5$ for this material. The tensile yield stress of this material was found to be 101 MPa and 165 MPa at 293°K and 253°K, respectively, which is 0.0717 and 0.0966 times the shear modulus at these respective temperatures. The machined tubular specimens were not annealed further but were given a featureless finish on both inside and outside surfaces by polishing with 0.1μm gamma alumina and were subsequently provided with a controlled roughness on their outside surfaces by touching the centers of spinning specimens for 10 seconds with wet polishing cloth bearing 4μm sized SiC particles. This produced grooves typically of a depth of 0.1 - 0.25μm [33]. The topography of such roughened surfaces was measured for reference by interference microscopy from high resolution metal replicas of the surface [33,34]. The aspect ratios k of the primary micro-grooves obeyed roughly a normal distribution. Secondary roughness along grooves, the presence of which could only be inferred by comparing experimental results with theory, could not be reliably measured.

Experiments were conducted on a specially constructed tension-torsion machine, the details of which are described elsewhere [34], in which it was eventually possible to limit the spurious interaction between the two modes of loading to about 1%. In spite of all the care in controlling specimen dimensions, concentricity, surface roughness, and machine cross interactions, reproductibility of experimental results was at best only within a factor of 2 in craze density or craze time (see the data for $s = 25.51$ MPa, $\sigma = 12.41$ MPa at 253°K in Figure 8c). Increases in surface density of crazes with time were measured photographically by using a technique of total reflection of light from craze interfaces [34]. Such film records were also used to determine craze growth rates under multi-axial stress. Multi-axial craze initiation and growth experiments were carried out both at 293°K. In addition, craze growth experiments were also performed in tension in thin sheets of commercial polystyrene ($M_w = 3 \times 10^5$, $M_n = 9 \times 10^4$) and polymethyl-methacrylate ($M_w = 2.46 \cdot 10^6$, $M_n = 2.52 \times 10^5$) which were machined into narrow guage length specimens, annealed, and polished with 0.1 μm gamma alumina to suppress stray craze nucleation. These specimens, however, were not specially roughened. They always contained sufficient numbers of imperfection from which a light density of crazes could nucleate. These commercial materials must have contained unknown additives. Craze growth measurements under tension in such commercial grade materials were again made by photographic recording of craze length at both 293°K and 253°K.

Craze Initiation

Figures 7a, b, c and 8a, b, c give the measured increase in surface craze density (number of crazes per cm^2 as a function of time at 293°K and 253°K, respectively, for different combinations of nominal (global) deviatoric

*We are grateful to Dr. C. Arends of Dow Chemical Company of Midland, Michigan for kindly supplying us with this material.

stress and negative pressure in the specimens manufactured from the DOW 686 type polystyrene. The curves are theoretical results which will be discussed below. The data shows that at a given negative pressure an increase in deviatoric stress gives an increase in the craze density for a given time, and produces eventually a higher density of crazes at which saturation occurs. The same is true for an increase in negative pressure at constant deviatoric stress (see data for s = 17.92 MPa in Figures 7a, 7b and 7c). The behavior at 253°K and 293°K are rather similar, except that the levels of stress for a given craze nucleus density at a given time are much higher at 253°K. In each instance the observed crazes were always perpendicular to the maximum principal tensile stress. The visual appearance of surfaces where crazing ceased suggested that craze interference had taken place stopping not only the nucleation of new crazes but also slowing down and even stopping the growth of established crazes.

Craze Growth

Figures 9a,b, and 10 show examples of craze length as a function of time in commercial PS and PMMA at 293°K and 253°K. In a large number of other similar measurements only constant rates of craze growth were observed under a constant stress as long as the craze remained intact and as long as crazes did not interfer. All cases of observed craze deceleration were attributable to craze interference on surfaces that had reached craze densities near saturation levels. In Figure 11 the results of all of these measurements of terminal craze velocity for both 293°K and 253°K are plotted against the 5/6th power of the ratio of the applied tensile stress to the athermal tensile flow stress $\hat{Y}$ at the respective temperatures. The straight lines represent the least square fits to the experimental data. Note that Figure 11 contains also the data from the DOW 686 type PS from a large selection of different multi-axial stress states showing that in this case the normalized maximum principal tensile stress governs the craze growth rate.

DISCUSSION

Craze Initiation

The theory on craze initiation presented earlier requires knowledge of considerable amount of molecular and microstructural detail in addition to some bulk material parameters such as the yield stress and shear modulus at the test temperatures. The majority of this information is available either in the form of additional data from yield experiments [42] or from the literature. There remains, however, some other parameters that cannot be determined readily by independent experiments and are too model-sensitive for theoretical computation. These include the relative shear displacement ϕ in equations (1) and (2), the microstructural heterogeneity spacing L in equation (2), the effective average aspect ratio $\bar{k}$ of the surface grooves and the effective standard deviation σ_k of these aspect ratios appearing in equation (11), the actual level of Q, the reduction factor of the effective plastic resistance to plastic hole growth when a deviatoric stress is present, that appears in equation (7) et sec, the actual magnitude of the pre-exponential factor $\dot{\beta}_o$ in equation (6) et sec, and the total integrated surface density of crazable sites N_o in equation (11). Therefore, these parameters have not been fixed *ab initio*. Instead their best-fit values have been determined by systematically fitting the theory to the experimental results. The magnitudes of these operational parameters have then been compared with expected ranges of values and were all found to be quite satisfactory. This, however, makes the theory

somewhat less than fully predictive, but gives an invaluable mechanistic insight into crazing and suggests methods by which the crazing process can be affected. Below we summarize how the values of the remaining parameters can be determined by a systematic procedure. A more detailed discussion of this procedure can be found elsewhere [44,46].

The knee in the N vs t curves given in Figures 7 and 8 are convenient references. The pairs of N, t values at the knee were plotted on log-log coordinates for the deviatoric stress s = 17.92 MPa at the three negative pressures of 2.07, 4.14, 6.21 MPa, respectively. Since the local deviatoric stress is constant for a given craze density (given aspect ratio k of grooves), given global deviatoric stress, and given global negative pressure, any change in the logarithm of the crazing time at constant N and global s gives directly the coefficient Q which was found to be 0.0133 indicating that in the yielded material at the tips of surface grooves the "effective" plastic resistance to hole growth had dropped down to 1.3% of its value in the absence of a local deviatoric stress.

The craze density N depends only on the aspect ratios k of the grooves from which crazes nucleate. Considering that the pore initiation time t_{in} given in equation (8) usually makes up most of the craze initiation time, as long as the negative pressure is not too small, an initial evaluation of $(1/\dot{\beta}_o)\exp(\alpha L^3 Y/kT)$ is possible. It was shown earlier [33] that at 293°K the first term of the activation free energy for pore nucleation is, in units of kT,

$$\frac{\Delta G_{pore} - \alpha L^3 Y}{kT} = \frac{(0.15)^2\,\pi(\mu/s)(\mu\phi^3)}{kT} = 9.545/(s/Y) \qquad (19)$$

where $s(k,\eta,\xi)$, the local deviatoric stress has been normalized for convenience with respect to the tensile yield stress Y at room temperature. Thus, since the craze initiation time at the knee in the curves in Figures 7a,b,c is roughly 2×10^2 sec a straight forward evaluation of equation (8) gives that $\ell n(\dot{\beta}_o \exp(-\alpha L^3 Y/kT)) \simeq 13$. Based on this initial choice of 13, as well as for 14 and 15, values of k were computed from the actual values of η, ξ, and t for the knees of the curves in Figures 7a,b,c. These were then plotted against the saturation values N_{sat} for each of the trial values of 13, 14, and 15 for $\ell n(\dot{\beta}_o \exp(-\alpha L^3 Y/kT))$. The best fit shown in Figure 12 confirmed that the initial choice of 13 gives the least spread in the data on N_{sat}. If the density of crazable sites obeys a normal distribution in k as suggested by equation (11), then the best curve passing through the points in Figure 12 should satisfy the equation

$$\frac{k - \bar{k}}{\sqrt{2}\,\sigma_k} = \sqrt{\ell n\left[\frac{N_o}{\sigma_k\sqrt{2\pi}}\right] - \ell n\left[-\frac{dN}{dk}\right]} \qquad (20)$$

Thus, the correct choice of

$$\ell n\left[\frac{N_o}{\sigma_k\sqrt{2\pi}}\right]$$

should give a linear plot between k and the function under the square root sign of equation (20). Such a choice is 12.523, with the use of which $\bar{k}$ and σ_k can be obtained from the intercept and slope of this line. This final fit shown by the solid curve in Figure 12 is given by $N_o = 1.782 \cdot 10^5$ cm^{-2}, $\bar{k} = 1.35$, and $\sigma_k = 0.259$. The theoretical fit is completed by

obtaining the actual saturation levels of craze density where craze interference takes place. This is readily achieved by using in equations (12a, b) the measured craze growth rate for 293° for the DOW 686 PS given in Figure 11, for which the best fit of the form of equation (17) is,

$$\frac{da}{dt} = \frac{4.192 \cdot 10^{-11}}{(\xi + \eta)} \exp\left[30(\xi + \eta)^{5/6}\right] \quad \text{cm/sec.} \tag{21}$$

The final levels of craze saturation shown in Figures 7a,b,c are obtained for a value $f \simeq 10^{-4}$ in equation (12b), which is far shorter than full coverage of the surface with crazes. Part of the reason for such a low level for f may lie in a missed scale factor in the measured velocity of equation (21). On the other hand, actual observations confirmed that in all cases nucleation of new craze sites ceases far sooner than craze growth does, indicating that after the most severe grooves have been used up in craze production the times of nucleation of new crazes from lesser grooves are significantly increased by small reductions of local stress from crazes growing in the vicinity.

Using the values for the factors of $\ell n(\dot{\beta}_o \exp(-\alpha L^3 Y/kT))$, N_o, $\bar{k}$, σ_k, Q and f that were established by fitting the theory to the data at 293°K, and the experimental craze growth rate information in Figure 11 for DOW 686 PS, the N vs. t curves for 253° can now be calculated. To obtain the fit shown in Figures 8a, b, and c it was found necessary to shift all these curves along the time axis by a constant amount which finally fixes $\alpha L^3 = 3.983 \cdot 10^{-22}$ cm^3 and $\dot{\beta}_o = 4.643 \cdot 10^{11}$ sec^{-1}. If α, which is the product of the average hole relaxation strain after a microcrack is formed, and the ratio of the hole to the heterogeneity spacing, is taken as 0.1, then the size of the hole and hence the heterogeneity spacing is found to be of order 1.6×10^{-7} cm. Then the magnitude of the frequency factor $\dot{\beta}_o$ which is expected to be related to the molecular segment frequency of $\sim 10^{13}$ sec^{-1} by the ratio of ϕ/L is also found to have the appropriate magnitude.

Comparison of the theoretical curves with the experimental data in Figures 7 and 8 shows that although there is no systematic deviation there are considerable departures from what could be considered a good fit. These departures result from: unavoidable eccentricities in the specimens, unavoidable low level spurious coupling between the tension and torsion devices, a below-than-normal distribution of the grooves with large stress concentration and random variation of the actual distribution in each specimen from the overall average. In spite of these random departures in the fit between the experimental results and the theory, the latter reproduces all the features of the experiments to a very satisfactory level.

Bi-axial Craze Initiation Locus

It is of interest to present the craze initiation theory and the experimental results as a craze initiation locus in the bi-axial principal stress plane of σ_1/Y and σ_2/Y (or in the ξ, η plane), as has been pioneered by Sternstein and co-workers [6-8]. Although such loci have been given many times [6-8, 9] the exact criterion of what is considered a craze-yield stress has never been well defined. In our theory several different criteria are possible. A criterion which corresponds to a visually detectable level at a given time, such as e.g. the locus of stresses ξ, and η for a craze density of $N = 10^4$ cm^{-2} at a time of $t = 10^2$ sec would come close to what has been initially used by Sternstein et al [6]. Such a bi-axial craze initiation locus can be obtained by equating the total craze nucleation time in equation (10) to 10^2 sec, substituting k = 1.76

(obtained from Figure 12) in equation (8), setting $m = (\partial \ell n \dot{\gamma}/\partial \ell n \tau)_T$ to 24 (see [42]) and finally substituting equations (8) and (9) into equation (10). This gives for the equation of the bi-axial craze initiation locus

$$\frac{(A/SQ)}{(\xi/Q)} - (\xi/Q) - \ell n\left[1 - \left(\frac{0.6}{(\xi/Q)}\right)^{24}\right] = C \tag{22}$$

where A is the coefficient of $(s/Y)^{-1}$ in equation (19) (A = 9.545 at 293°K and 9.310 at 253°K), C = 21.23 at 293°K and 12.70 at 253°K is a combination of numerical factors that results from the substitutions mentioned above, the constant 0.6 is obtained from the evaluation of the integral in equation (9), and finally

$$s(\eta/\xi, k) = \left\{\frac{1}{3}\left[(1 - \eta/\xi)^2 - (0.096k + 1)(1 - (\eta/\xi)^2) + (1.262k^2 + 1.992k + 1)\left(1 + \frac{\eta}{\xi}\right)^2\right]\right\}^{1/2} \tag{23}$$

is obtained from equation (4) by factoring out ξY. In equation (23), of course, k is to be set equal to 1.76 corresponding to $N = 10^4$ cm^{-2}, and in equation (22) Q is to be taken at 0.0133 as determined earlier above. The craze initiation loci at T = 293°K and 253°K, obtained from equation (22) are plotted in Figure 13, together with the six data points obtainable from Figures 7 and 8 corresponding to the time levels of applied negative pressure in these experiments. The agreement, as could be expected by virtue of the previous fit, is very good. The third curve shown in Figure 13 is for a groove aspect ratio of k = 0.5 corresponding to what may be expected to be found on the surface of a "well protected" PS sheet. These curves which approach the pure shear axis closely at levels significantly below yield differ considerably from those presented by Sternstein and co-workers [6-8]. Although the exact reason for this departure is not clear, a possible explanation for the room temperature results may be the relatively lower crazing resistance of the additive-free DOW 686 PS which was used in our study. The higher craze velocities shown in Figure 11 for this material at T = 293° may be an indication of this. This explanation, of course, would not hold for the T = 253° results.

Craze Growth

Figure 11 shows that craze growth for the three polymers tested obeys the simple expression given by equation (17). The slopes and levels of these lines give the exponent $(A/T)\lambda_n^{5/6}$ and the pre-exponential constant (D/λ_n) $\exp(-A/T)$ of the velocity of craze growth. These values are tabulated in Table I, together with the calculated values of D, using the appropriate magnitudes of the physical properties and derived functions given in equation (18), which are also listed. From these exponents and pre-exponential constants the experimental values of A/T and λ_n have been calculated and are also listed in Table I, together with the computed values of A/T based on equation (15b) where the appropriate values of molecular parameters were used that have been obtained from the temperature dependence of the plastic shear resistance of these polymers [42]. The values of the natural draw ratios λ_n of the polymers in craze matter obtained from the slopes and levels of the data shown in Figure 11 could not be compared with any theoretical model. Examination of the experimental magnitudes of (A/T) and λ_n show that the values of DOW 686 PS at 253°K are clearly out of line. The computed value for $\lambda_n = 0.614$ indicating compression rather than extension of the craze matter is impossible. The strange behavior of this material at 253°K is also evident from Figure 11. Since no unusual

temperature dependence of the yield behavior of this polymer was noted [34], and the use of the experimentally obtained craze growth behavior of this polymer gave very satisfactory correlation of the saturation behavior of crazing in this material at 253°K, as was discussed in connection with Figure 8, spurious errors in the measurement of craze velocities must be ruled out. The possibilities that remain are: a bi-axial residual compressive stress in the surface layers of the tension torsion specimens resulting from a thin surface layer of higher coefficient of expansion, or an unusual strain hardening behavior in the craze tip plastic zone of the DOW 686 PS at 253°K. Aside of this unusual behavior of the DOW 686 PS, comparison of the experimental values of A/T with the theoretical prediction show that these are in a ratio of 0.72 for both PS's at 293°K and 0.52 for 253° for the commercial PS, while the ratio is 0.8 at 293° for PMMA. The major part of this reduction of the experimental values of A/T must be related to the significant lowering of the shear modulus in a glassy polymer by a negative pressure. In PS, e.g., the ratio of the plastic shear resistance in tension to the plastic shear resistance in compression is 0.71 [48], which is almost exactly of the same magnitude as the ratio of the A/T values listed in the last row of Table I. Although no information is available for the strength differential effect in PS at 253°K, the difference at this temperature in the A/T values is probably too large to be explained entirely by the effect of negative pressure on modulus and other effects, such as strain hardening in the craze tip plastic zone, probably play an important role.

Analogy Between Crazing and Ductile Fracture

The mechanism of craze nucleus formation that has been discussed has much in common with ductile fracture in metals where more or less localized plastic flow produces large stress concentrations on interfaces of heterogeneities, particles, and inclusions that produce holes. These holes subsequently grow together by plastic flow and result in rupture by rapid localization of this cavitation process. We have postulated here that similiar disturbances in the plastic flow of polymers occur by molecular heterogeneities. Since the stress concentrations required to bridge between the plastic resistance and the cohesive strength in glassy polymers is only of the order of 3-5, only relatively mild variations in plastic resistance is necessary. Although the exact nature of these variations is not clear in the flexible chain polymers, such as PS and PMMA, (in distinction to inflexible chain polymers, such as polyimides [47]), they must be a result of variations in molecular packing. Whatever their source, such inhomogeneities in plastic flow at a near molecular level have been observed to develop and form cavities in thin films [25,26] that lends support to our mechanism. The development of a craze nucleus in the yielded material by the interaction of a critical volume fraction of holes at surface grooves where localized plastic flow has occurred has been modelled purely on the basis of continuum plasticity which should be applicable at this scale. This process in bulk material would be difficult to follow. Yet, the many detailed low angle x-ray diffraction measurements of Zhurkov and co-workers [31,32] on cavitation in stressed glassy polymers comes very close to a direct verification of this process.

At some stage soon after the craze nucleus has formed and has acquired a significant aspect ratio normal to the maximum principle tensile stress, it can grow by the faster mechanism of craze matter production involving the meniscus instability. Comparison of the kinetics of craze growth by hole nucleation with that of the meniscus instability shows that the former has a much steeper stress dependence and at the usual levels of crazing

stress can only give craze growth rates that are many orders of magnitude lower than experimentally measured rates [44]. On the other hand, at high stress levels, near general yield, the hole nucleation mechanism would appear to dominate the growth of crazes -- even though none of the reported measurements of craze growth rate exhibit this type of stress dependence. Some support for this possibility, however, comes from fracture experiments neat T_g where the plastic resistance is low, the velocity of craze growth just preceding the propagation of the crack is immeasurably high. In such experiments, electron fractography of the split craze structure has shown evidence of considerable independent nucleation of holes [40,46]. This could, however, also have resulted from the process of splitting of craze matter described by Murray and Hull [11] that occurs after the craze has formed. In comparison, the mechanism relying on the meniscus instability appears on firm ground. Not only do the kinetics match the observed ones but also the topology giving continuously connected air passages and the scale of the predicted craze structure are in order. For the latter, Argon and Salama [46] predict a wavelength λ of the instability that must give the spacing of the craze tufts, as

$$\lambda = 12\pi^2 A(1/m) \chi\sqrt{3}/Y \qquad (24)$$

where $A(1/m)$ is a computed function of the strain rate sensitivity m of the medium ($A(1/m) \sim 1.5$ for $m \geq 15$) and all other quantities are as defined earlier. For a surface energy $\chi \simeq 5 \times 10^{-2}$ J/m^2 and a tensile plastic resistance of $Y \simeq 10^2$ MPa, λ is 0.14 μm which for an extension ratio $\lambda_n \simeq 2$ of craze matter gives a craze tuft diameter of 0.05 μm that is right in the range of what is usually observed with electron microscopy.

The crazing theory which we have summarized here is based on as detailed mechanisms as we find currently possible to give, consistent with known experimental measurements and molecular detail. Future research on crazing in oriented polymers and polymers with radically different molecular flexibility, such as polyimides, may make further refinements possible.

ACKNOWLEDGEMENT

For stimulating discussion throughout several years we are particularly grateful to Professor F. A. McClintock, Dr. R. Kambour, and Professor I. M. Ward, in whose laboratory at the University of Leeds this work initiated during a sabatical leave. This work has been supported by the National Science Foundation under Grants GH-40467, DMR 73-02440-A01, and through the Center of Materials Science and Engineering at M.I.T. under Grant DMR 72-03027-A05.

REFERENCES

1. RABINOWITZ, S. and BEARDMORE, P., CRC Critical Reviews in Macromolecular Science, eds. E. Baer, et al., CRC Press, Cleveland, 1, 1972, 1.
2. KAMBOUR, R. P., J. Polymer Sci.: Macromolecular Reviews, 7, 1973, 1.
3. MAXWELL, B. and RAHM, L. F., J. Soc. Plastics Eng., 6, 1950, 7.
4. BUCKNALL, C. B. and SMITH, R. R., Polymer, 6, 1965, 437.
5. BOWDEN, P. B. and OXBOROUGH, R. J., Phil. Mag., 28, 1973, 547.
6. STERNSTEIN, S. S., ONGCHIN, L. and SILVERMAN, A., Applied Polymer Symposia, 7, 1968, 175.
7. STERNSTEIN, S. S. and ONGCHIN, L., Polymer Preprints, 10(2), 1969, 117.

8. STERNSTEIN, S. S. and MYERS, F. A., J. Macromol. Sci-Phys. B8(3-4), 1974, 539.
9. OXBOROUGH, R. J. and BOWDEN, P. B., Phil. Mag., 30, 1974, 171.
10. HAWARD, R. N., MURPHY, B. M. and WHITE, E. F. T., in Fracture 1969, ed. P. L. Pratt, Chapman and Hall, London, 1969, 519.
11. MURRAY, J. and HULL, D., J. Polymer Sci., Part A-2, 8, 1970, 583; and 8, 1970, 1521.
12. DOYLE, M. J., MARANCI, A., OROWAN, E. and STORK, S. T., Proc. Roy. Soc., A329, 1972, 137.
13. BERNIER, G. A. and KAMBOUR, R. P., Macromolecules, 1, 1968, 393.
14. MARSHALL, G. P., CULVER, L. E., WILLIAMS, J. G., Proc. Roy. Soc., A319, 1970, 165.
15. ANDREWS, E. H. and BEVAN, S., Polymer, 13, 1972, 337.
16. WILLIAMS, J. G. and MARSHALL, G. P., Proc. Roy. Soc., A342, 1975, 55.
17. WILLIAMS, J. G., MARSHALL, G. P., GRAHAM, I. and ZICHY, E. L., Pure and Applied Chemistry, 39(1-2), 1974, 275.
18. PARRISH, M. and BROWN, N., J. Macromol. Sci-Phys., B8(3-4), 1974, 655.
19. OLF, H. G. and PETERLIN, A., Polymer, 14, 1973, 78.
20. KAMBOUR, R. P. and HOLIK, A. S., J. Polymer Sci., Part A-2, 7, 1969, 1393.
21. BEAHAN, P., BEVIS, M. and HULL, D., Phil. Mag., 24, 1971, 1267; J. Mater. Sci., 8, 1972, 162.
22. KAMBOUR, R. P. and KOPP, R. W., J. Polymer Sci., Part A-2, 7, 1969, 183.
23. HOARE, J. and HULL, D., Phil. Mag., 26, 1972, 443.
24. BRADY, T. E. and YEH, G. S. Y., J. Macromol. Sci-Phys., B7(2), 1973, 243.
25. WELLINGHOFF, S. T. and BAER, E., in Yield, Deformation and Fracture of Polymers (outlines of lecture presentations at the 2nd Intern. Conf. on Yield, Deformation and Fracture, Churchill College, Cambridge), Plastics Institute, London, 1973, 3-1.
26. WELLINGHOFF, S. T. and BAER, E., J. Macromol. Sci-Phys., B11(3), 1975, 367.
27. NARISAWA, I. and KONDO, T., Intern. J. Fracture Mech., 8, 1972, 435.
28. GENT, A. N., J. Mater. Sci., 5, 1970, 925.
29. ARGON, A. S., J. Macromol. Sci-Phys., B8(3-4), 1973, 573.
30. VERHEULPEN-HEYMANS, N. and BAUWENS, J. C., J. Mater. Sci., 11, 1976, 7.
31. ZHURKOV, S. N., KUKSENKO, V. S. and SLUTSKER, A. I., in Fracture 1969, eds. P. L. Pratt, et al., Chapman and Hall, London, 1969, 531.
32. ZHURKOV, S. N., VETTEGREN, V. I., KORSUKOV, V. E. and NOVAK, I. I., in Fracture 1969, eds. P. L. Pratt, et al., Chapman and Hall, London, 1969, 545.
33. ARGON, A. S., Pure and Applied Chemistry, 43(1-2), 1975, 247.
34. HANNOOSH, J. G., Craze Initiation in Glassy Polymers, Ph.D. Thesis, Dept. Mech. Eng., M.I.T., Cambridge, Mass., 1975.
35. BESSONOV, M. I. and KUVSHINSKII, E. V., Soviet Physics-Solid State, 3, 1961, 950.
36. NARISAWA, I. and KONDO, T., J. Polymer Sci. (Phys.), 11, 1973, 223.
37. VERHEULPHEN-HEYMANS, N. and BAUWENS, J. C., J. Mater. Sci., 11, 1976, 1.
38. KRAMER, E. J., KRENZ, H. G. and AST, D. G., submitted to Phil. Mag.
39. KNIGHT, A. C., J. Polymer Sci., A3, 1965, 1845.
40. SALAMA, M. M., Craze Growth in Glassy Polymers, Sc.D. Thesis, Dept. Mech. Eng., M.I.T., Cambridge, Mass., 1975.
41. STROH, A. N., Proc. Roy. Soc., A223, 1954, 404.

42. ARGON, A. S., Phil. Mag., 28, 1973, 839; in Polymeric Materials, Relationship Between Structure and Mechanical Behavior, ASM, Metals Park, Ohio, 1975, 411.
43. NEUBER, H., Theory of Notch Stresses, J. W. Edwards, Ann Arbor, Michigan, 1946, 108, 126.
44. ARGON, A. S. and HANNOOSH, J. G., (to be published).
45. McCLINTOCK, F. A. and STOWERS, I. F., Research Memorandum No. 159, Fatigue and Plasticity Laboratory, M.E. Dept., M.I.T., Cambridge, Mass., 1970.
46. ARGON, A. S. and SALAMA, M. M., Materials Sci. Eng., 23, 1976, 219; (to be published).
47. ARGON, A. S. and BESSONOV, M. I., Phil. Mag., in press.
48. ARGON, A. S., ANDREWS, R. D., GODRICK, J. A. and WHITNEY, W., J. Appl. Phys., 39, 1968, 1899.

Table I Experimental and Theoretical Parameters for Craze Growth in PMMA and Two Types of PS

	PMMA	PS		DOW 686 PS	
	293K	253K	293K	253K	293K
$(A/T)\lambda_n^{5/6}$	96.34	69.35	74.76	26.62	94.95
$(D/\lambda_n)\exp(-A/T)$ m/sec	4.58×10^{-18}	7.27×10^{-16}	5.66×10^{-15}	1.95×10^{-12}	5.14×10^{-15}
(A/T), expmtl	47.90	46.92	44.72	39.98	44.52
λ_n, expmtl	2.313	1.5983	1.853	0.614(?)	2.4815
B(1/m) [46]	3	2.4	2.4	2.4	2.4
$\chi/\dot{Y}$, m	1.773×10^{-10}	1.812×10^{-10}	1.812×10^{-10}	1.812×10^{-10}	1.812×10^{-10}
$\dot{\epsilon}_o$, sec^{-1} [42]	1.86×10^{11}	0.93×10^{13}	0.93×10^{13}	0.93×10^{13}	0.93×10^{13}
D, theory m/sec	6.76×10^{3}	2.77×10^{5}	2.77×10^{5}	2.77×10^{5}	2.77×10^{5}
(A/T), theory	60.22	81.67	62.16	81.67	62.16
$\frac{(A/T),\ \text{expmtl}}{(A/T),\ \text{theory}}$	0.80	0.52	0.72	0.49	0.72

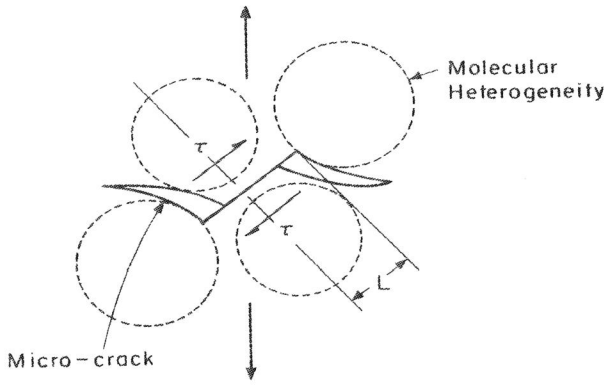

Figure 1 Formation of micro-cracks by arrest of micro-shear bands (from [33], courtesy of Butterworths).

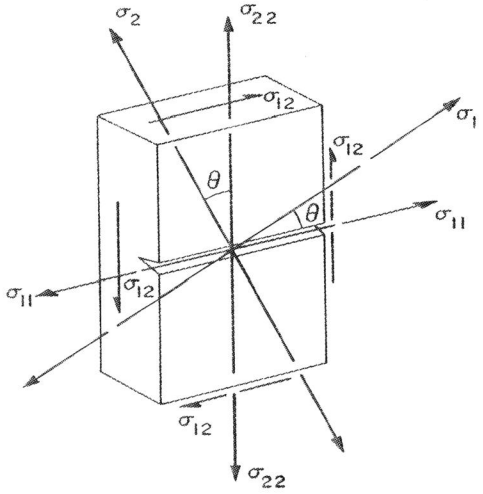

Figure 2 Surface groove under the application of a bi-axial state of stress (from [33], courtesy of Butterworths).

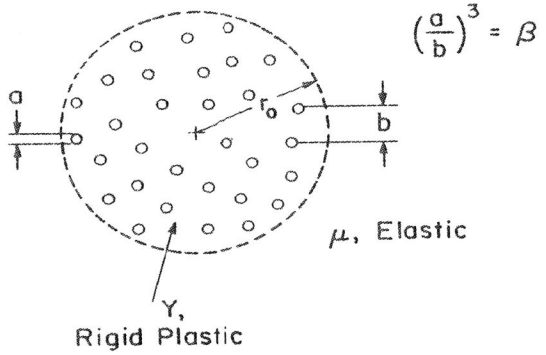

Figure 3 Porous rigid plastic region about to undergo cavitation under the action of a negative pressure applied by stressed elastic surroundings (from [33], courtesy of Butterworths).

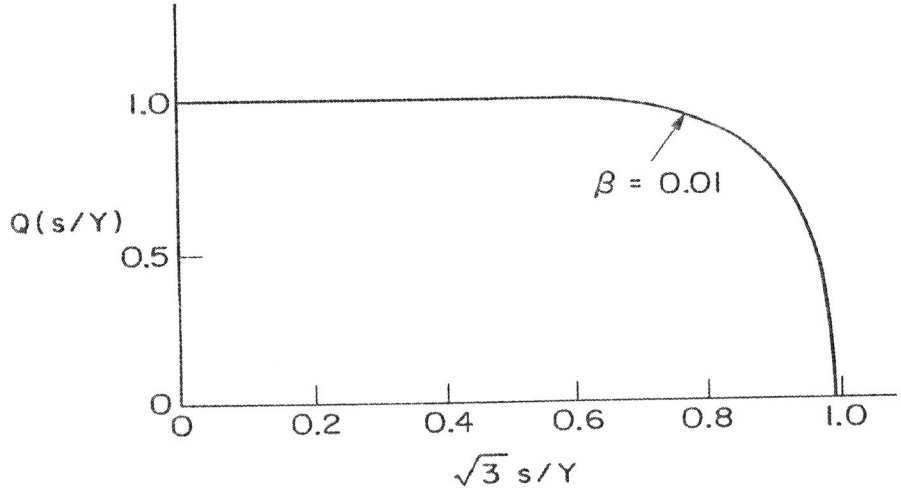

Figure 4 Locus of pore expansion under a combined negative pressure and deviatoric stress (after McClintock and Stowers [45]).

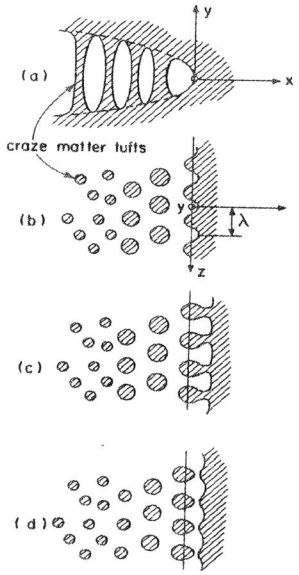

Figure 5 Schematic rendering of craze matter production by the mechanism of meniscus instability: a) outline of a craze tip, b) cross section in the craze plane across craze matter tufts, c), d) advance of the craze front by a completed period of interface convolution.

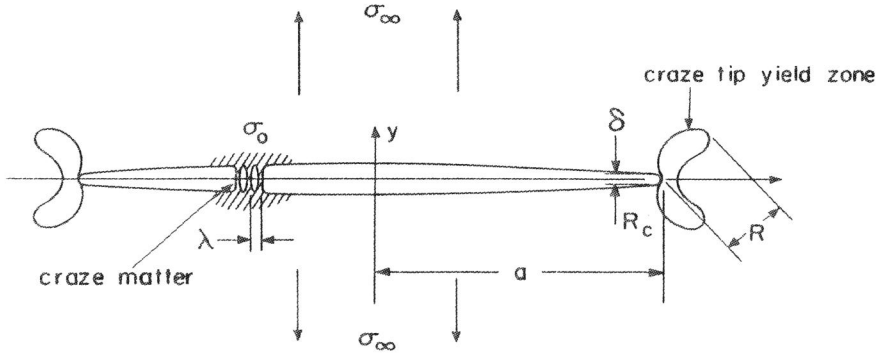

Figure 6 Craze as a planar yield zone; showing craze tip plastic zone, craze tip opening displacement and radius of curvature, and craze matter producing craze face traction.

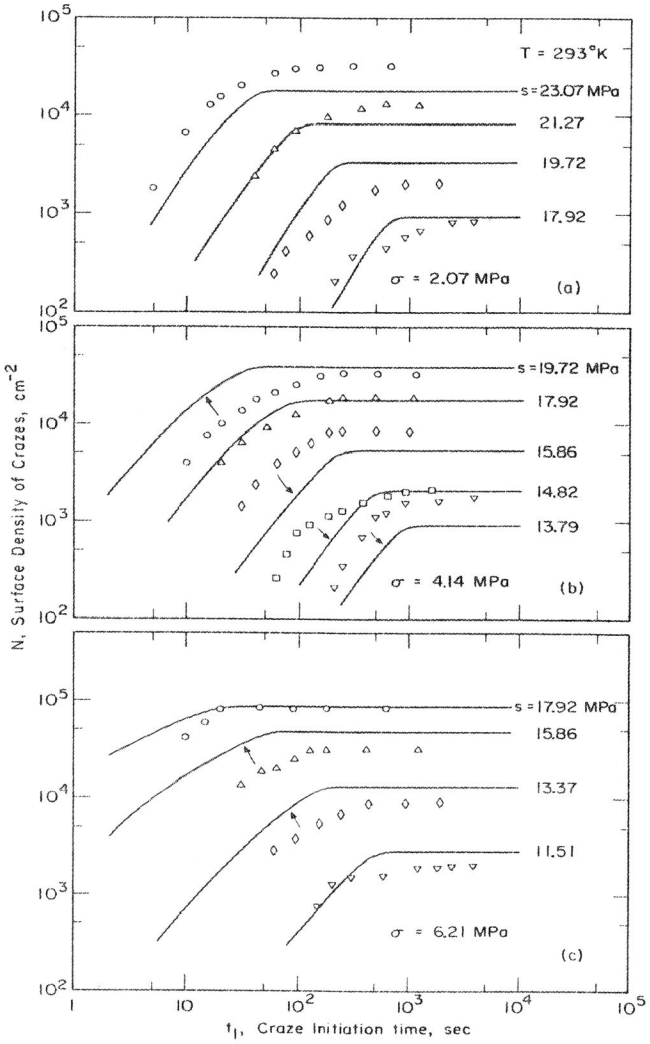

Figure 7 Increase of craze nuclei with time in samples subjected to different combinations of global deviatoric stress and negative pressure at room temperature. Curves computed using equations (8), (11) and (12b).

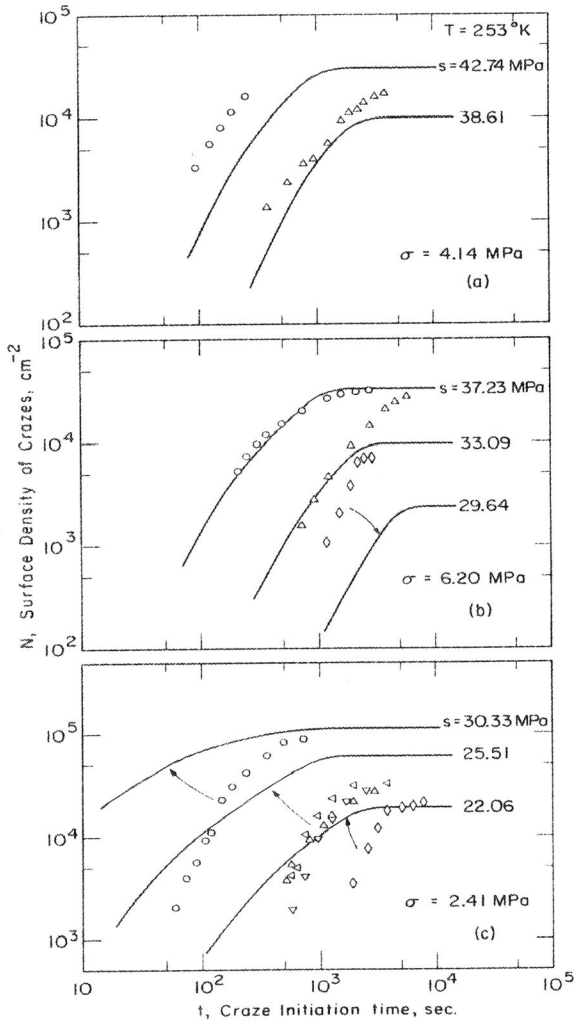

Figure 8 Same as preceding figure except at 235°K.

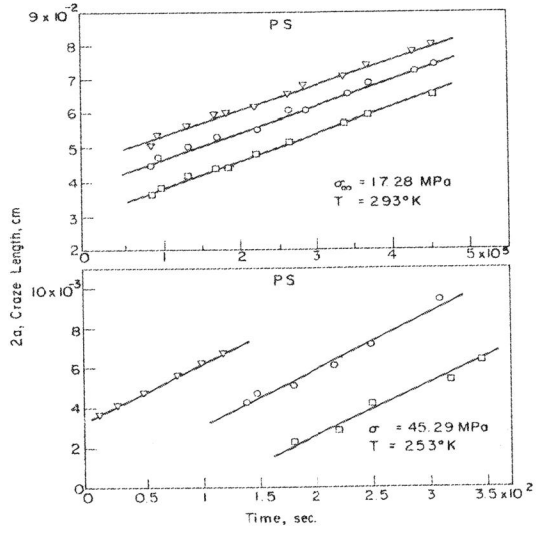

Figure 9 Examples of non-interfering craze growth in commercial PS under two different levels of stress and at two different temperatures. Lines are best fits to the data.

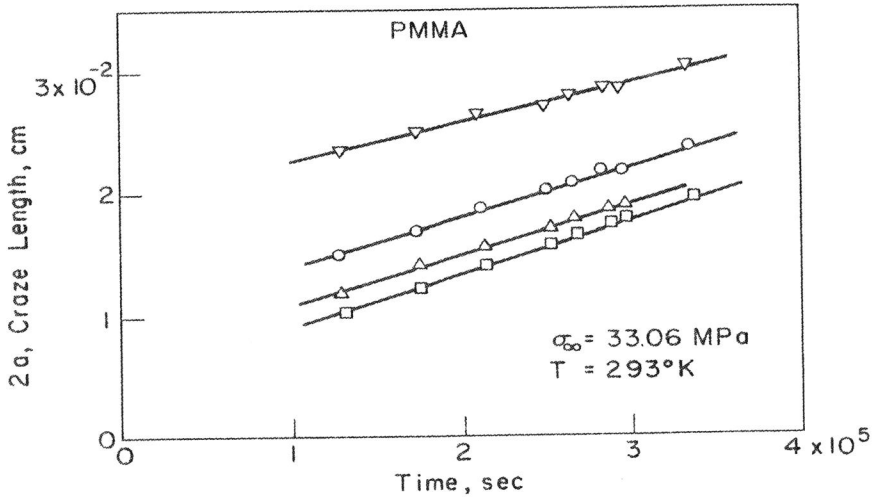

Figure 10 Examples of non-interfering craze growth in commercial PMMA under one stress level at room temperature.

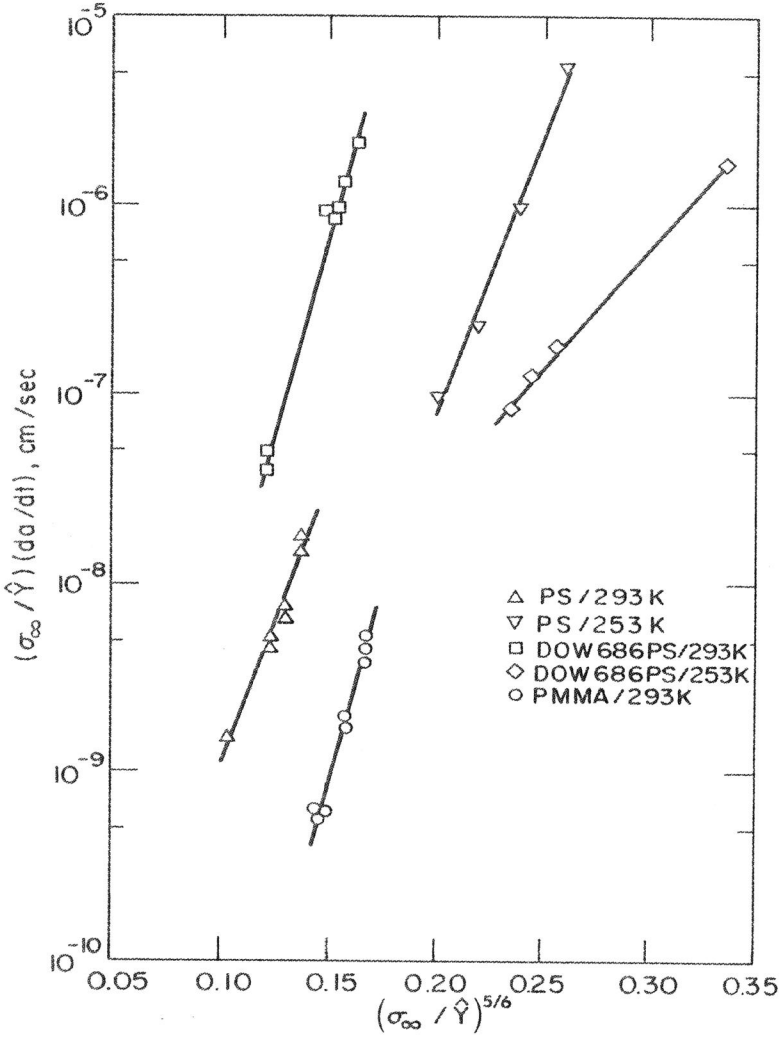

Figure 11 Dependence of normalized craze velocity on normalized maximum principle tensile stress at two temperatures for both commercial PS and DOW 686 PS (free of additives), and for commercial PMMA.

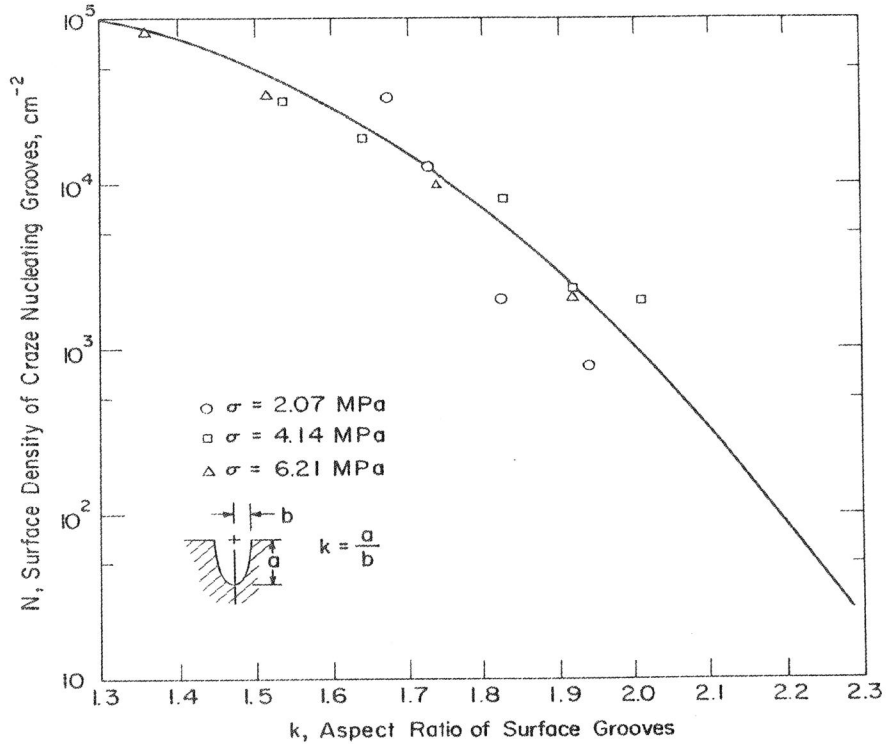

Figure 12 Density of potential craze producing surface sites on the DOW 686 PS specimens as a function of groove aspect ratio. Data points represent the saturation craze densities at room temperature given in Figure 7. The scale of the horizontal axis, as well as the best fitting normal distribution shown by the solid curve, have been obtained by a systematic fit discussed in the text.

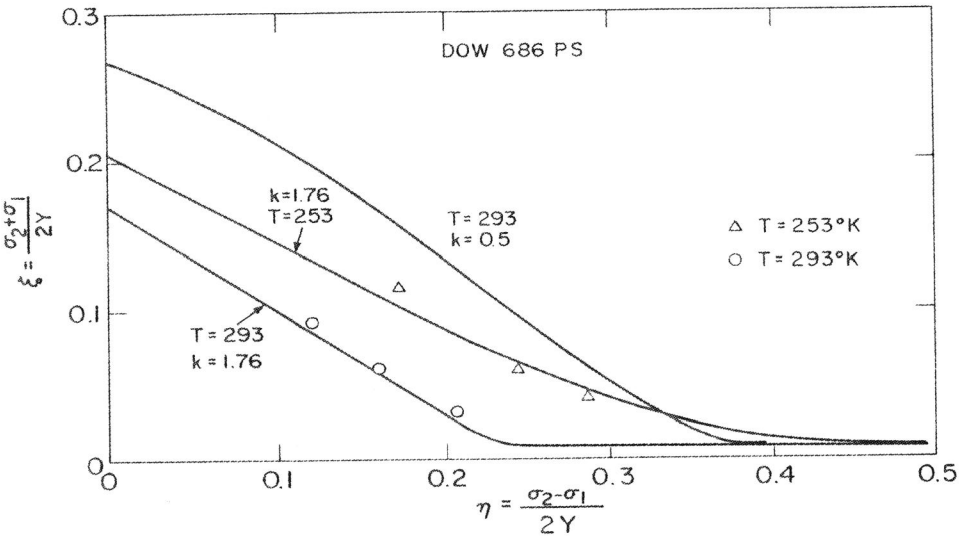

Figure 13 Bi-axial craze locus representing normalized stresses η, and ξ for a craze density of 10^4 sites/cm^2 in 100 seconds, for the DOW 686 PS, at 293°K and 253°K. The other solid curve is computed for a hypothetical PS with higher surface perfection.